RESEARCH ARTICLE

Particle & Particle Systems Characterization
www.particle-journal.com

Controllable Preparation of Nanosized $LiMnPO_4$/C with Rod-Like Morphology by Hydrothermal Method with Excellent Electrochemical Performance

*Da-Jun Zhang, Shao-Hua Luo, and Jun Zhang**

The nanosized rod-like $LiMnPO_4$/C cathode materials have successfully in situ synthesized on the surface of flaky structure $MnPO_4 \cdot H_2O$ self-sacrificing template by the hydrothermal method. The crystal microstructure, micro shape, and electrochemical parameters of $LiMnPO_4$/C are comprehensively studied by XRD, SEM, TEM, and electrochemical measurement methods. The physical and chemical properties analysis confirms that the vinyl acetate solution (VAc-H_2O) with a proper molar ratio is beneficial to generate orthorhombic olivine structure $LiMnPO_4$ with microporous structure and nanorod-shaped morphology. The electrochemical measurement results indicate that LMP-X1-AA sample delivers an initial discharge capacity of 148.1 mAh g^{-1} at 0.05 C, the capacity retention rate still maintains at 89.2% after 200 cycles. As the discharge rate increases to 1 C, the discharge capacity still remains at 133.4 mAh g^{-1}. The results indicate that the synergistic effect of nanosized rod-like morphology and conductive carbon coating is beneficial to improving the lithium ions diffusivity and electrochemical properties of $LiMnPO_4$ materials.

1. Introduction

With the dramatical development of energy storage devices, lithium-ion batteries (LIBs) have extensively become an influential power supply source of portable electronic devices, new-energy automobiles, and intelligent power grid applications on account of the high-energy density, long service life, quick charge, and excellent safety features.[1–4] Intensive researches illustrate the properties of cathode electrodes mainly influence the economy, security, and electrochemical performance of LIBs. For the sustainability of energy supply, a series of cathode materials, like layered structure $LiCoO_2$, olivine structure $LiFePO_4$ and ternary materials have been widely developed and researched.[5] Compared with structurally different cathode materials, polyanionic-based $LiMnPO_4$ material has deemed to be a potential cathode electrode on account of the merits in high specific energy density (700 Wh kg^{-1}), good structural stability, high operating voltage platform (4.1 V vs Li/Li^+), superior safety, low price, abundant Mn resources, environmental friendliness and compatible with the existing electrolytes system.[6–9] However, the internal intrinsic structure drawbacks of $LiMnPO_4$ give rise to poor electronic conductivity, sluggish Li-ion diffusion rate, and severe Jahn-Teller effect of Mn^{3+} in the host structure, which results in inferior electrochemical performance and further restrict large mass production.[10,11] Many modification methods have been applied to resolve the issues, including morphology and size controlling,[12–15] cation doping,[16–19] and carbon coating.[20–23] Generally, the grain size/morphology controlling and carbon coating have been found influential to facilitate the rapid Li-ion migration velocity and enhance the electrochemical properties of $LiMnPO_4$/C. Ragupathi et al.[12] have proved the performance improvement of $LiMnPO_4$/C is ascribed to the synergistic effect of nanopyramids like morphology and conductive carbon coating by increasing the Li-ion diffusion kinetics, $LiMnPO_4$/C exhibits an initial discharge capacity of 164.2 mAh g^{-1}, and 130.8 mAh g^{-1} after 500 cycles at 0.1 C. The influence of multiple nanoscale shapes $LiMnPO_4$ on tap-density and Li-ion diffusion path/direction have been studied by Kwon et al.,[15] they confirm the performance improvement is attributed to large specific surface area and the shortened lithium ions diffusion distance in $LiMnPO_4$ nanoparticles. Guo et al.[20] have reported the nanosized plate-like shape $LiMnPO_4$ shows excellent cycling stability and rate capability, the carbon-coated sample exhibits a high discharge capacity of 104 mAh g^{-1} at 10 C. Recently, Zhang Group[24] has synthesized tunable morphologies $LiMnPO_4$/C nanocrystals varying the feeding sequence and the ratio of the reactants in an EG-assisted solvothermal approach, the results confirm that excess LiOH amount is indeed required to yield $LiMnPO_4$ crystals with small particle size and attractive electrochemical properties. Cao group[25] develop a heating reflux method to synthesize dumbbell-like $MnPO_4 \cdot H_2O$ hierarchical particle using $KMnO_4$ and H_3PO_4 as raw materials, and then

D.-J. Zhang, J. Zhang
College of Pharmacy
Shenyang Medical College
Shenyang 110034, People's Republic of China
E-mail: zhangjun@symc.edu.cn
S.-H. Luo
School of Resources and Materials
Northeastern University at Qinhuangdao
Qinhuangdao 066004, People's Republic of China

The ORCID identification number(s) for the author(s) of this article can be found under https://doi.org/10.1002/ppsc.202300019

DOI: 10.1002/ppsc.202300019

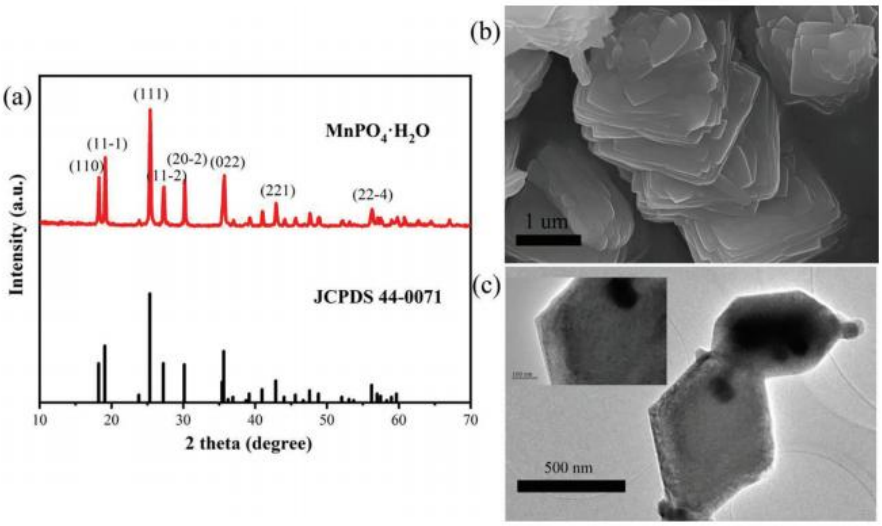

Figure 1. The data of the $MnPO_4 \cdot H_2O$ precursor. a) XRD diffraction pattern; b) SEM photograph; c) TEM image.

employed as the precursor to prepare $LiMnPO_4$/C composites. The synthesized $LiMnPO_4$/C exhibits good electrochemical performance, which shows a potential application for the large-scale synthesis of $LiMnPO_4$ cathode materials. Therefore, the strategies of regulating grain size/micromorphology and carbon coating could effectively improve the electrochemical performance by shortening the lithium ions diffusion distance and improving the electronic/ionic conductivity of $LiMnPO_4$ materials.

In our work, we adopt the co-precipitation method to prepare flaky structure $MnPO_4 \cdot H_2O$ precursor, and then nanosized $LiMnPO_4$/C cathode materials with rod-like morphology are synthesized by the hydrothermal method in different VAc-H_2O ratio mixture solvents. The synergistic effect of nanosized rod-like morphology and conductive carbon coating on the microstructure, grain size, crystal morphology, and electrochemical parameters of $LiMnPO_4$/C materials have been comprehensively investigated.

2. Experimental Section

2.1. Materials Synthesis

The nanosized $LiMnPO_4$/C were synthesized by the hydrothermal method in different ratio vinyl acetate solution (VAc-H_2O), using $LiOH \cdot H_2O$, $Mn(NO_3)_2$, and H_3PO_4 as raw reagents. All the raw reagents were analytically pure and commercially available without further purification. To study the influence of the crystal microstructure and surface morphology on electrochemical lithium storage features of $LiMnPO_4$, the contrast experiments were conducted by maintaining all parameters the same and regulating VAc-H_2O ratio and carbon coating condition.

$MnPO_4 \cdot H_2O$ precursor was synthesized by the precipitation method. For the synthesis process, a stoichiometric amount of H_3PO_4 and $Mn(NO_3)_2$ were respectively dissolved in the ethyl acetate solvent (H_2O-EA) to form a uniform solution. The $MnPO_4 \cdot H_2O$ precursor was precipitated by dropping a certain concentration of H_3PO_4 into $Mn(NO_3)_2$ mixture solution under vigorous stirring for 1 h at a bathing temperature of 50 °C, the reactions were started to nucleate and generate precipitates gradually. After the precipitation reaction, the dark green $MnPO_4 \cdot H_2O$ precipitates were obtained after washing, centrifuging with deionized water and alcohol for three times, then dried at 80 °C in the air for 8 h.

The chemical synthesis procedures of $LiMnPO_4$/C were described as follows. First, $LiOH \cdot H_2O$ and $MnPO_4 \cdot H_2O$ with a molar ratio of 1:1 were successively dissolved in a different volume ratio of VAc-H_2O mixture solutions, and kept continuously stirring for 1 h to form the uniform mixture. The prepared mixture solution was transferred to the autoclave with Teflon-lined volume of 50 ml. After being reacted at 160 °C for 10 h, the $LiMnPO_4$ precursor precipitates were gathered after washing, centrifuging with deionized water and anhydrous alcohol for three times, then drying at 80 °C for 12 h in air conditions. The $LiMnPO_4$/C precursor was blended and ground with 25 wt.% ascorbic acids in the ethanol dispersion medium, then calcined at 550 °C for 3 h under nitrogen gas atmosphere, finally the target $LiMnPO_4$/C cathode materials were obtained. The products prepared in pure water system, in pure VAc system, in VAc-H_2O (v/v = 1:2), in VAc-H_2O (v/v = 2:1), were named as LMP-W, LMP-VAc, LMP-X1, LMP-X2, The ascorbic acid coated LMP-X1, and LMP-X2 samples were named as LMP-X1-AA and LMP-X2-AA.

2.2. Physical Characterization

The crystalline microstructure was characterized by X-ray diffractometer (XRD, Rigaku Smartlab) with Cu Kα radiation under a sweep speed of 0.04° s^{-1} in the range of 10–80°. The crystal grain size, micromorphology, element distribution, and carbon layer structure were detected by scanning electron microscopy (SEM, ZEISS SUPRA55) equipped with the X-ray energy

dispersive spectroscopy (EDS) and transmission electron microscopy (TEM, JEOL JEM2100F).

2.3. Electrochemical Measurements

The electrochemical behaviors of $LiMnPO_4$/C cathodes were evaluated by CR2032 coin cells, which were assembled in the argon gas filled glovebox. The cathode slurry was prepared by dispersing the active material, PVDF binder, and acetylene carbon black in the NMP dispersant in a mass ratio of 8:1:1 with vigorous stirring for 4 h. The slurry was coated on the Al foil and dried at 80 °C for 8 h in air condition, aiming to volatilize the NMP solvent. Then, the foil was pressed and cut into a circular slice with 1 cm in diameter. Before the assembling of CR2032 coin cells, the prepared electrode slices were drying at 120 °C for 12 h in the vacuum condition to ensure the bond dry and used as the cathode electrode. In CR2032 coin cells, metallic lithium wafer, Celgard 2400 membrane, and 1 M $LiPF_6$/DEC+MEC+EC (volume ratio = 1:1:1) solution were served as the anode electrode, separator, and electrolytes, respectively.

The electrochemical charge/discharge measurements were tested on the battery tester (CT2001A, Land) using the test voltage range of 2.5 V–4.5 V at different discharge rates. Electrochemical impedance spectroscopy (EIS) was recorded on the electrochemical workstation (1260+1287 type, Solartron) to analyze the charge transfer resistance on the interface of the active material and electrolytes at 10 mV voltage amplitude, and the test frequency was from 10^{-1} to 10^5 Hz. All the electrochemical measurements were under ambient conditions.

3. Results and Discussion

The flake shape $MnPO_4{\cdot}H_2O$ precursor has been synthesized by the precipitation method, the crystal structures are investigated by XRD. **Figure 1**a shows the XRD pattern of $MnPO_4{\cdot}H_2O$, the main diffraction peaks are in good agreement with the standard card JCPDS 44–0071 of $MnPO_4{\cdot}H_2O$. The intensity of diffraction peaks is high and the half-peak width is narrow, indicating the grains size is large. Meanwhile, no impurity peaks are detected, which indicates the complete crystalline structure and high purity of $MnPO_4{\cdot}H_2O$ sample. Figure 1b displays the SEM photograph of the $MnPO_4{\cdot}H_2O$ precursor, the $MnPO_4{\cdot}H_2O$ precursor shows flake shape with length and width in the range of 1.5–2.0 μm, and all the flake shapes overlap together and form layered structure. The TEM image of $MnPO_4{\cdot}H_2O$ is shown in Figure 1c, which further confirms the overlapped flaky structure of $MnPO_4{\cdot}H_2O$ precursor.

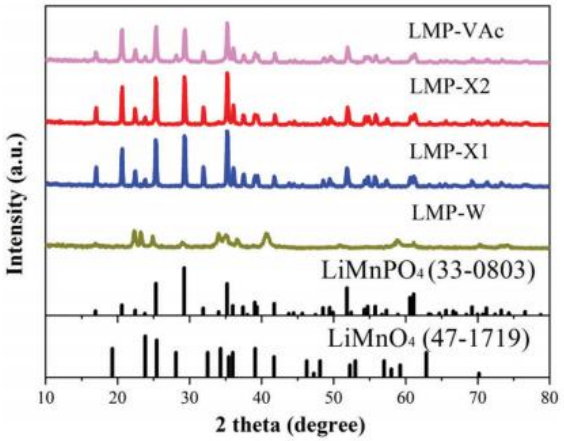

Figure 2. XRD diffraction patterns of as-prepared samples.

Figure 2 shows the XRD diffraction patterns of $LiMnPO_4$ samples. The X-ray diffraction spectra manifest that the olivine-type

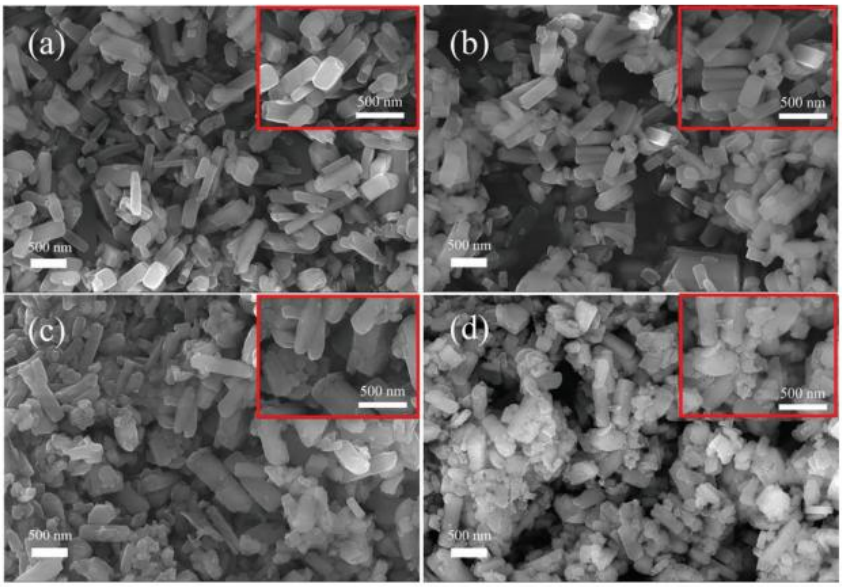

Figure 3. SEM micrographs of $LiMnPO_4$ samples, inert is the magnification images. a) LMP-X1; b)LMP-X2; c) LMP-X1-AA; d) LMP-X2-AA.

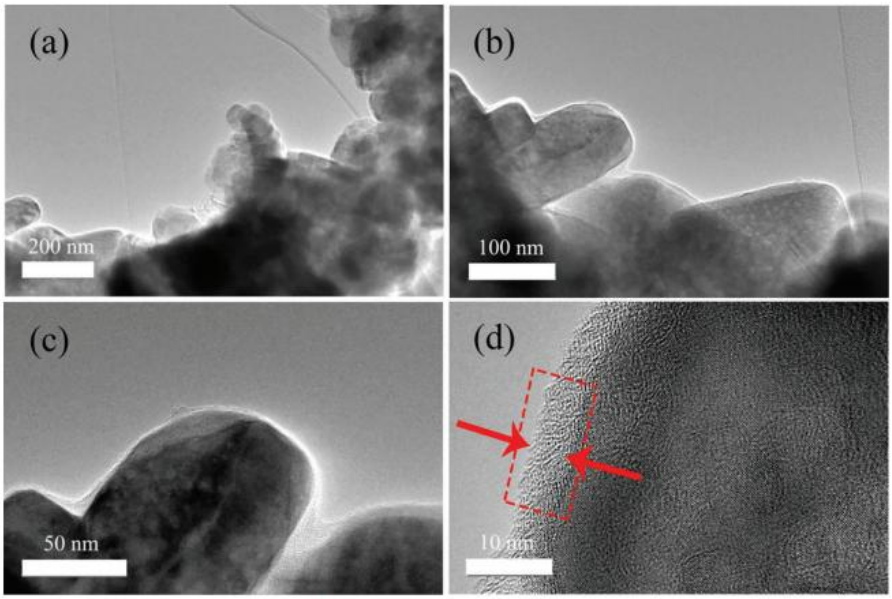

Figure 4. TEM photographs of LMP-X1-AA sample under different magnifications.

$LiMnPO_4$ could not synthesize in pure water. In the pure VAc solvent system, the impurity phase $LiMnO_4$ (47–1719) has been found. The olivine structure $LiMnPO_4$/C in the orthorhombic space have been synthesized in different VAc-H_2O (v/v = 1:2 or 2:1) mixture solvent system. It is observed that the sharp characteristic diffractive peaks of LMP-X1 and LMP-X2 samples are indexed well with the standard card (JCPDS 33–0803) of $LiMnPO_4$, and no impurity and carbon diffraction peaks are found, which confirm the orthorhombic crystalline structure and the purity of as-prepared $LiMnPO_4$ samples. Based on XRD analysis, we can conclude that the pure phase $LiMnPO_4$ materials could synthesize in different VAc-H_2O ratio mixture solvents system, the composition of solvent plays a critical role in the stability of crystal structure of $LiMnPO_4$ samples.

Figure 3 shows the SEM micrographs of the prepared $LiMnPO_4$ samples. The typical morphologies of LMP-X1 and LMP-X2 samples are depicted in Figure 3a,b. It is observed that the samples show rod-like shape hollow structure and inconsistency size with 354–571 nm in length and 65–200 nm in width, all the nanorods pile up together and form a uniform porous structure. As the volume ratio of VAc-H_2O is 1:2, the LMP-X1 sample shows relatively higher porosity and uniform dispersion. With the volume ratio keep increasing, the agglomeration phenomenon becomes serious. The results indicate the volume ratio of VAc-H_2O (v/v = 1:2) plays an important role in obtaining rich pore structure to ensure a sufficient contact area across the interface of the active material and electrolyte and decrease the Li-ion diffusion path. As can be seen in Figure 3c,d, after the carbon coating process, the grains size and morphology of the samples seem similar to the uncoated samples, the pyrolysis carbon is uniformly distributed on the surface of $LiMnPO_4$ nanorods, which construct a good conductive network.

Figure 4 displays the TEM photographs of LMP-X1-AA sample. It could be observed that numerous nanorods with a length and width over 70 nm stack tightly together. From the high-magnification TEM photograph in Figure 4d, we can see the continuous carbon layer is uniformly adhered to the outer surface of the nanorods with a thickness of 4–6 nm, constructing a good electronic conductive network structure. The conductive carbon layer is obtained by the pyrolysis of ascorbic acid, which could facilitate the electronic transfer and storage ability of the cathode materials.

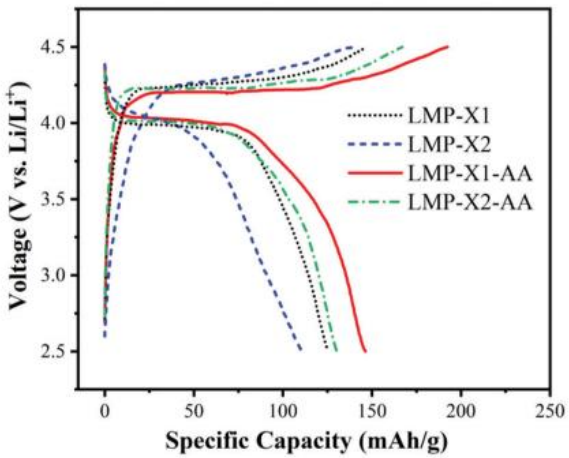

Figure 5. The charge/discharge curves of LMP-X1, LMP-X2, LMP-X1-AA, and LMP-X2-AA samples for the first cycle.

The charge/discharge measurements of as-prepared $LiMnPO_4$/C samples have been tested at 0.05 C on the coin cells. **Figure 5** shows the first charge/discharge curves of LMP-X1, LMP-X2, LMP-X1-AA, and LMP-X2-AA samples, showing a flat discharge voltage platform ≈4.0 V, corresponding

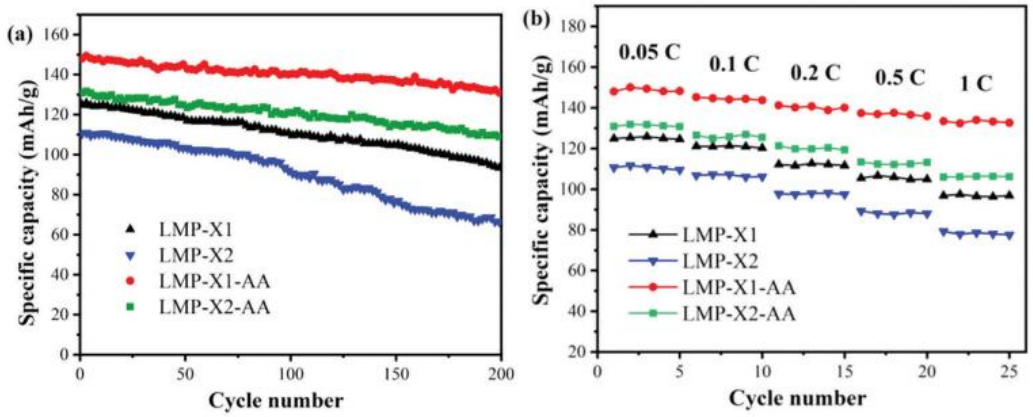

Figure 6. The electrochemical performance of LMP-X1, LMP-X2, LMP-X1-AA, and LMP-X2-AA samples. a) Cycling ability; b) Rate performance.

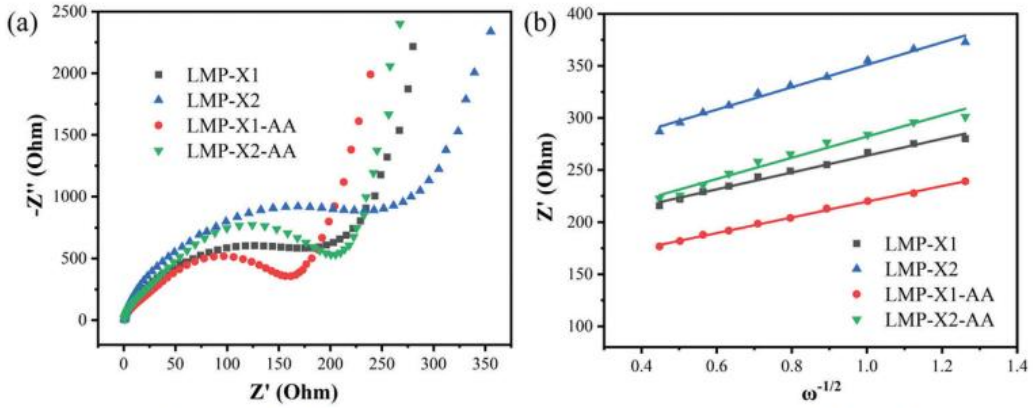

Figure 7. a) The EIS plots of LMP-X1, LMP-X2, LMP-X1-AA, and LMP-X2-AA samples; b) The linear fitting line between Z' and $\omega^{-1/2}$ at low-frequency region.

to the Mn^{3+}/Mn^{2+} redox reaction during the Li-ion insertion/deinsertion process. LMP-X1 delivers higher discharge capacity than that of LMP-X2, indicating the different crystal growing environments greatly influence the variation tendency of the discharge-specific capacity of $LiMnPO_4$ samples. From the charge/discharge curves, we can see the voltage difference between the charging and discharging platform for LMP-X1-AA sample is smaller than other samples, indicating the low polarization of LMP-X1-AA. Meanwhile, LMP-X1-AA sample exhibits longer discharge voltage plateau and higher discharge capacity of 148.1 mAh g^{-1}, which indicate that a certain amount of carbon coating could effectively accelerate the electron conductivity to enhance the electrochemical storage performance.

The cycling stability and rate performance of all the samples have been tested by the galvanostatic charge/discharge measurements. The cycling performance of all the samples is measured at 0.05 C discharge rate for 200 cycles, the cyclic curves are displayed in **Figure 6**a. After 200 cycles, the capacity retention rate of LMP-X1, LMP-X2, LMP-X1-AA, and LMP-X2-AA decrease to 74.5%, 59.2%, 89.2%, and 83.26%, respectively. The results indicate that conductive carbon coating is a resultful way to improve the cycle performance of the cathode materials. Figure 6b shows the rate performance curves of all the samples discharging from 0.05 C to 1 C. The discharge capacity of LMP-X1-AA decreases slightly from 148.1 mAh g^{-1} (0.05 C) to 145.3 mAh g^{-1} (0.1 C), 137.3 mAh g^{-1} (0.5 C), respectively. The LMP-X1-AA sample still exhibits excellent rate capacity with the discharge capacity value of 133.4 mAh g^{-1} even at 1 C. However, LMP-X2 sample shows the worst discharge-specific capacity and cycle performance. The excellent electrochemical performance of LMP-X1-AA sample indicates the lithium ions migration rate is fast across the nano-sized $LiMnPO_4$ with rod-like morphology to shorten the lithium ions diffusion distance.

The EIS test was employed to discuss the charge transport kinetics properties on the interface between active electrode materials and the electrolytes. **Figure 7**a shows the Nyquist plots of LMP-X1, LMP-X2, LMP-X1-AA, and LMP-X2-AA samples, the Nyquist plots are made up of two sections, including a semicircular shape in the high-middle frequency region, and an oblique line in the low-frequency region. The intercept of the semicircles at the axis of real is corresponding to the interfacial charge transfer resistance (R_{ct}). The slope of the straight line signifies

the Warburg impedance of the Li-ion diffusion (W_o). Compared with all the samples, LMP-X1-AA with smaller semicircle diameter delivers lower R_{ct} value, indicating the carbon coating modification could greatly improve the electrochemical reaction kinetics during the delithiation/lithiation process. Moreover, the Li-ion diffusion coefficient (D_{Li}^+) of all the samples have been calculated by the following equation $D_{Li^+} = R^2T^2/2A^2n^4F^4C^2\sigma^2$and $Z' = R_s + R_{ct} + \sigma w^{-1/2}$, where T, R, n, F, A, C and σ are the absolute temperature, the gas constant, the number of electrons per molecule, Faraday constant, efficient contact area, the concentration of lithium-ion and the Warburg factor, respectively. As depicted in Figure 7b, the slope value (σ) of LMP-X1-AA is smaller than other samples. As a consequence, the calculated D_{Li}^+ value of LMP-X1-AA is larger than other samples. The lower R_{ct} value and larger D_{Li}^+ are contributed to improve the electrochemical performance and interfacial lithium ions transfer of $LiMnPO_4$ cathode materials, which are in agreement with the charge/discharge measurement analysis conclusions.

4. Conclusions

In our work, nanosized rod-like $LiMnPO_4$ cathode materials have been successfully in-situ synthesized on the surface of flaky shape $MnPO_4{\cdot}H_2O$ precursor by the hydrothermal method in the VAc-H_2O (v/v = 1:2) mixture solvent system. After carbon coating process, LMP-X1-AA sample exhibits the discharge capacity of 148.1 mAh g^{-1} at 0.05 C, 145.3 mAh g^{-1} at 0.1 C, and 133.4 mAh g^{-1} at 1 C, respectively. After 200 cycles, the capacity retention rate maintains at 89.2%. The physical and chemical measurements illustrate the existence of orthorhombic olivine structure $LiMnPO_4$ with the nanorod and carbon layer morphology. The electrochemical results clarify the nanorod shape morphology and conductive carbon coating are beneficial to improve electrochemical properties of $LiMnPO_4$/C cathode materials.

Acknowledgements

The work was funded by the National Natural Science Foundation of China (No.52104307, No.51874079, No.51674068), Liaoning Province Ordinary Higher Education Institutions Intercollegiate Cooperation Project (No.202010), Liaoning Province Education Department Science and Technology Research Project (No.SYYX202014), Scientific Research Fund of Shenyang Medical College (No.20201006), Science and Technology Fund of Shenyang Medical College (No.20195076), Natural Science Foundation of Liaoning Province (No. 2020-MS-313).

Conflict of Interest

The authors declare no conflict of interest.

Data Availability Statement

Research data are not shared.

Keywords

electrochemical performance, $LiMnPO_4$, lithium-ion batteries, rod-like structures

Received: January 31, 2023
Revised: March 10, 2023
Published online:

[1] Y. Wan, Q. J. Zheng, D. M. Lin, *Acta. Chim. Sin.* **2014**, *72*, 537.
[2] S. H. Luo, Z. L. Tang, J. B. Lu, Z. T. Zhang, *Ceram. Int.* **2008**, *34*, 1349.
[3] J. N. Zhu, W. C. Li, F. Cheng, *J. Mater. Chem. A* **2015**, *3*, 13920.
[4] S. Luo, D. Hu, H. Liu, J. Li, T. F. Yi, *J. Hazard. Mater.* **2019**, *368*, 714.
[5] L. Liang, W. Zhang, F. Zhao, D. K. Denis, F. Zaman, L. R. Hou, C. Z. Yuan, *Adv. Mater. Interfaces* **2019**, *7*, 901749.
[6] L. Liang, X. Sun, J. Zhang, *Adv. Energy Mater.* **2019**, *9*, 1802847.
[7] L. Bao, Y. Chen, G. Xu, T. Yang, *Eur. J. Inorg. Chem.* **2018**, *13*, 1533.
[8] T. Lv, H. Min, H. B. Shu, Y. J. Zhou, Q. Q. Liang, *Electrochim. Acta* **2020**, *359*, 136945.
[9] S. Y. Li, N. W. Li, C. W. Sun, *Inorg. Chem. Front.* **2021**, *8*, 361.
[10] L. Esmezjan, D. Mikhailova, M. Etter, J. Cabana, C. P. Grey, S. Indris, H. Ehrenberg, *J. Electrochem. Soc.* **2019**, *166*, A1257.
[11] I. Bezza, M. Kaus, R. Heinzmann, *J. Phys. Chem. C* **2015**, *119*, 9016.
[12] V. Ragupathi, P. Panigrahi, G. S. Nagarajan, *Appl. Surf. Sci.* **2019**, *495*, 143541.
[13] N. H. Kwon, H. Yin, T. Vavrova, *J. Power Sources* **2017**, *342*, 231.
[14] D. Choi, D. Wang, I.-T. Bae, J. Xiao, *Nano Lett.* **2010**, *10*, 2799.
[15] X. Pan, Z. Gao, L. Liu, *J. Alloys Compd.* **2019**, *783*, 468.
[16] A. Gutierrez, R. Qiao, L. Wang, *Chem. Mater.* **2014**, *26*, 3018.
[17] P. Gibot, M. Casas-Cabanas, L. Laffont, *Nat. Mater.* **2008**, *7*, 741.
[18] L. W. Liang, X. Sun, J. Y. Zhang, L. R. Hou, J. F. Sun, Y. Liu, S. G. Wang, C. Z. Yuan, *Adv. Energy Mater.* **2019**, *9*, 1802847.
[19] K. P. Wu, S. Yin, S. Wang, J. L. Zhu, W. T. Yao, *Carbon* **2020**, *169*, 55.
[20] H. Guo, C. Y. Wu, L. H. Liao, J. Xie, *Inorg. Chem.* **2015**, *54*, 667.
[21] Y. Hong, Z. L. Tang, S. T. Wang, W. Quan, Z. T. Zhang, *J. Mater. Chem.* **2015**, *A3*, 10267.
[22] J. Z. Li, S. H. Luo, Q. Wang, *Electrochim. Acta* **2018**, *289*, 415.
[23] J. Song, J. Gim, S. Kim, W. Park, *J. Nanosci. Nanotechnol.* **2015**, *15*, 6053.
[24] Y. Hong, Z. L. Tang, W. Quan, S. T. Wang, Z. T. Zhang, *Ceram. Int.* **2016**, *42*, 8769.
[25] Y. Z. Wang, G. R. Hu, Z. D. Peng, K. Du, B. C. Zhang, Y. B. Cao, *Ceram. Int.* **2021**, *47*, 19687.